Spatiotemporal change of sky polarization during the total solar eclipse on 29 March 2006 in Turkey: polarization patterns of the eclipsed sky observed by full-sky imaging polarimetry

Brigitta Sipőcz, Ramón Hegedüs, György Kriska, and Gábor Horváth*

Department of Biological Physics, Biooptics Laboratory, Physical Institute, Eötvös University, H-1117 Budapest, Pázmány sétány 1, Hungary

*Corresponding author: gh@arago.elte.hu

Received 20 September 2007; revised 30 November 2007; accepted 3 December 2007; posted 4 December 2007 (Doc. ID 87795); published 30 May 2008

Using 180° field-of-view (full-sky) imaging polarimetry, we measured the spatiotemporal change of the polarization of skylight during the total solar eclipse on 29 March 2006 in Turkey. We present our observations here on the temporal variation of the celestial patterns of the degree p and angle α of linear polarization of the eclipsed sky measured in the red (650 nm), green (550 nm), and blue (450 nm) parts of the spectrum. We also report on the temporal and spectral change of the positions of neutral (unpolarized, $p = 0$) points, and points with local minima or maxima of p of the eclipsed sky. Our results are compared with the observations performed by the same polarimetric technique during the total solar eclipse on 11 August 1999 in Hungary. Practically the same characteristics of celestial polarization were encountered during both eclipses. This shows that the observed polarization phenomena of the eclipsed sky may be general. © 2008 Optical Society of America

OCIS codes: 010.1290, 110.2960, 120.5410, 280.1310.

1. Introduction

Piltschikoff [1] was the first to report that at the beginning of the totality of the solar eclipse on 30 August 1905 in Philippeville, Algeria, the degree of linear polarization p of skylight decreases drastically at 90° from the eclipsed Sun. Using point-source polarimetry, de Bary *et al.* [2] measured the polarization of an eclipsed sky. They observed the temporal change in p of skylight at 90° from the obscured Sun during the total solar eclipse of 15 February 1961 in Viareggio, Italy. Moore and Rao [3] registered the polarization at some points of the sky during the total eclipse on 30 May 1965 from an aircraft intercepting the Moon's shadow in the vicinity of Bellingshausen Atoll at an altitude of 12.3 km. Rao *et al.* [4] measured the degree of linear polarization of skylight at a few celestial points during the total eclipse on 12 November 1966 from an aircraft flying at an altitude of 10 km above the Uruguayan coast. Furthermore, Dandekar and Turtle [5] also performed point-source polarimetric measurements in the blue and red spectral ranges during the total eclipse of 7 March 1970 in Kinston, North Carolina, USA. Miller and Fastie [6] observed the skylight polarization during the total solar eclipse on 30 May 1965 from an aircraft flying at an altitude of 12.2 km over the South Pacific. Shaw [7] was the first who sequentially measured the celestial polarization at numerous points along two orthogonal lines on the skydome. Using a rotating-analyzer point-source polarimeter, he registered the polarization of skylight in the blue part of the spectrum in the solar vertical plane (i.e., the Sun's vertical) and in a vertical plane perpendicular to the solar meridian during the 30 June 1973 total eclipse in Kenya, Africa. Using two polarimeters oriented in the direction of the zenith and at 90° from the Sun in the Sun's vertical, Coulson [8] observed a virtual lack of polarization response during a partial (80%) eclipse

0003-6935/08/34000H1-10$15.00/0

of the sun at Davis, California, USA, on 26 February 1979. With the help of a numerical model, Können [9] quantitatively explained several polarization characteristics of the eclipsed sky, especially the occurrence of a neutral (unpolarized, $p = 0$) point near the zenith.

All these early measurements of the polarization of eclipsed skies were carried out by point-source polarimeters with fields of view not wider than a few degrees. The development of full-sky imaging polarimetry [10–14] and its use during total solar eclipses [15,16] resulted in a qualitative improvement in the study of the polarization pattern of the eclipsed sky. The forerunner of imaging polarimetry of the eclipsed sky was Gerharz [17], who took photographs about the celestial circumsolar area of $12° \times 15°$ through a modified Savart filter and a green interference filter during the total eclipse of 7 March 1970 near Williamston, North Carolina, USA. From the photographed interference bands he deduced the degree and angle of linear polarization of light scattered from the circumsolar region of the eclipsed sky.

Pomozi *et al.* [15] were the first who could measure the fine structure of the polarization pattern of an eclipsed sky. Using 180° field-of-view imaging polarimetry, they registered the spatiotemporal change of the polarization of the celestial hemisphere during the total solar eclipse of 11 August 1999 in Kecel, Hungary. They compared these patterns with the normal celestial polarization patterns measured at the same time on the day after the eclipse. As a second control sky, the celestial polarization pattern measured on 26 August 1999 in Tunisia was chosen with the same solar zenith angle (32°) as that during the Hungarian eclipse. They also investigated the spectral characteristics of sky polarization during totality in the red, green, and blue parts of the spectrum. They gave a qualitative explanation for the origin of the pattern of the angle of polarization and the neutral point of skylight polarization near the zenith observed during totality. Horváth *et al.* [16] reported on the observation of some neutral points and points with minimum p values in the eclipsed sky during the solar eclipse on 11 August 1999 in Kecel.

As far as we know, since the pioneering studies by Pomozi *et al.* [15] and Horváth *et al.* [16], the sky polarization during total solar eclipses have not been remeasured by full-sky imaging polarimetry. However, such studies would be important to reveal whether the polarization characteristics of the eclipsed sky and its neutral points observed by Pomozi *et al.* [15] and Horváth *et al.* [16] are particular or general. Until now no new comparative data have been published on the polarization patterns of the eclipsed sky. To fill this gap, using the same full-sky imaging polarimetric technique as those used by Pomozi *et al.* [15] and Horváth *et al.* [16], we measured the spatiotemporal change of the polarization of skylight during the total solar eclipse of 29 March 2006 in Turkey (Fig. 1). We present here our observations on the temporal variation of the celestial patterns of degree p and angle α of linear polarization and the positions of neutral (unpolarized, $p = 0$) points and points with local minima or maxima of p of the eclipsed sky in the red, green, and blue spectral ranges. During totality we were able to measure the celestial polarization patterns at eight different

Fig. 1. (Color online) Map of Turkey showing the path of the Moon's shadow (umbra) during the total solar eclipse on 29 March 2006. Our full-sky imaging polarimetric measurements were performed in the immediate vicinity of Side, the ancient maritime city on the coast of the Mediterranean Sea.

Table 1. Parameters of the Total Solar Eclipse on 29 March 2006[a]

Date of total solar eclipse	29 March 2006
Diameter ratio	1.0494
Eclipse obscuration	1.1013
Solar zenith angle	46°
Solar azimuth angle	204°
Velocity of the umbra along the path of totality	846 m/s
Major axis of the elliptical umbra	200 km
Minor axis of the elliptical umbra	164.1 km
Time of first contact (beginning of the partial eclipse)	12:38:22 (local summer time = UTC + 3)
Time of second contact (beginning of the total eclipse)	13:54:59
Time of midtotality	13:56:52
Time of third contact (end of the total eclipse)	13:58:44
Time of fourth contact (end of the partial eclipse)	15:13:34
Observation site	4 km from Side, Turkey, on the coast of the Mediterranean Sea
Latitude of observation site	36° 46′ N
Longitude of observation site	31° 23′ E

[a]Diameter ratio = $d_{\mathrm{Moon}}/d_{\mathrm{Sun}}$, eclipse obscuration = $A_{\mathrm{Moon}}/A_{\mathrm{Sun}}$, where d and A are the diameter and the area of the Moon's and the Sun's disk.

points of time. We gathered almost three times as much data on the polarization of the eclipsed sky as Pomozi *et al.* [15] and Horváth *et al.* [16], who could measure only at three points of time during totality. The theoretical interpretation and quantitative explanation of our observations by numerical simulations could be the task of future work.

2. Materials and Methods

All the relevant parameters of the total solar eclipse and the geographic coordinates and date of our imaging polarimetric measurements are summarized in Table 1. Our measurements were performed in Turkey, in the immediate vicinity of Side, the ancient maritime city, on the coast of the Mediterranean Sea (Fig. 1). This place was practically on the center line (the distance was only 4 km) of the path of the Moon's shadow (umbra) sweeping the Earth's surface. Fortunately, the atmosphere was clear and cloudless during our measurements from the beginning (first contact) to the end (fourth contact) of the partial eclipse.

The skylight polarization was measured by full-sky imaging polarimetry. The technique and evaluation procedure have been described in detail elsewhere [13]. A 180° field of view was ensured by a fish-eye lens (Nikon–Nikkor, $F = 2.8$, 8 mm focal length) with a built-in rotating disk mounted with three broadband (275–750 nm) neutral density linearly polarized filters (Polaroid HNPB) with three different polarization axes (0°, 45°, and 90° from the radius of the disk). The detector was a photoemulsion (either Kodak Elite Chrome ED 200 ASA, or Kodak EPH 1600 ASA; see Table 2) in a roll-film photographic camera (Nikon F801). The maxima and half-bandwidths of the spectral sensitivity curves of both detector types were $\lambda_{\mathrm{red}} = 650 \pm 40$ nm, $\lambda_{\mathrm{green}} = 550 \pm 40$ nm, and $\lambda_{\mathrm{blue}} = 450 \pm 40$ nm. For a given sky three photographs were taken for the three different directions of the transmission axis of the polarizers. The camera was set on a tripod so that the optical axis of the fish-eye lens was vertical, i.e., pointed to the zenith. After 24 bit (3×8 for red, green, and blue) digitization (by a Canon Arcus 1200 scanner) of the three chemically developed color pictures for a given sky and their computer evaluation, the patterns of radiance I, degree of linear polarization p, and angle of polarization α (measured clockwise from the local zenith meridian) of skylight were determined as color-coded, two-dimensional, circular maps. In these circular patterns the center is the zenith, the perimeter is the horizon, and the zenith angle θ is proportional to the radius from the zenith (zenith: $\theta = 0°$; horizon:

Table 2. Parameters of Recordings of the Full-Sky Imaging Polarimetric Measurements during the Solar Eclipse on 29 March 2006 in Turkey[a]

Number in Figs. 2–4[b]	Phase	Recording Time (UTC + 3)	Percent Obscuration of Sun's Disk (%)	Exposure Time (s)	Aperture (f number)	Photographic Film
1	Preeclipse	12:43:00	1.7	1/500	5.6	K200
2		13:47:00	87.9	1/250	2.8	K200
3		13:53:30	99.5	1/250	2.8	K1600
4	Eclipse (totality)	13:55:20	100	1	2.8	K1600
5		13:55:30	100	2	2.8	K1600
6		13:55:45	100	2	2.8	K1600
7		13:56:15	100	1	2.8	K1600
8		13:56:25	100	1	2.8	K1600
9		13:56:35	100	1	2.8	K1600
10		13:57:50	100	1	2.8	K1600
11		13:58:00	100	1	2.8	K1600
12	Posteclipse	14:06:00	88.5	1/250	2.8	K200
13		15:00:00	9.0	1/500	5.6	K200

[a]Color reversal films used were the following: K200 = Kodak Elite Chrome ED 200 ASA, K1600 = Kodak EPH 1600 ASA.
[b]Numbers 1–13 in the first column indicate the numbers of scenes in Figs. 2–4.

Table 3. Percentages[a]

Phase	Number in Figs. 2–4	k (%)			p (%)			n (%)		
		Red	Green	Blue	Red	Green	Blue	Red	Green	Blue
Preeclipse	1	70	72	72	19 ± 14	18 ± 13	17 ± 13	12	9	8
	2	59	65	69	19 ± 13	19 ± 13	18 ± 14	15	13	11
	3	57	60	60	20 ± 10	13 ± 7	11 ± 7	13	12	11
Eclipse (totality)	4	36	38	37	17 ± 8	15 ± 9	11 ± 5	17	12	9
	5	39	43	40	8 ± 5	6 ± 4	3 ± 2	10	9	15
	6	35	37	33	8 ± 5	7 ± 5	4 ± 2	14	10	14
	7	33	35	33	12 ± 6	12 ± 6	8 ± 4	21	17	16
	8	34	37	35	11 ± 6	11 ± 6	8 ± 4	21	17	15
	9	34	37	35	11 ± 6	11 ± 6	7 ± 4	20	18	15
	10	33	36	34	10 ± 6	10 ± 6	6 ± 5	23	20	17
	11	34	37	34	9 ± 6	9 ± 6	6 ± 4	23	17	19
Posteclipse	12	52	53	57	19 ± 14	20 ± 14	20 ± 15	16	11	11
	13	35	37	39	18 ± 13	19 ± 13	21 ± 15	18	13	10

[a] k (%) of the sky for which $45° \leq \alpha \leq 135°$ (from the local zenith meridian), degree of linear polarization p (%), and noisiness n (%) of the α-pattern of the sky during the total solar eclipse on 29 March 2006 measured by full-sky imaging polarimetry in Turkey in the red (650 nm), green (550 nm), and blue (450 nm) parts of the spectrum and averaged for the entire sky (average ± standard deviation).

$\theta = 90°$). These patterns were obtained in the red, green, and blue spectral ranges, in which the three color-sensitive layers of the photoemulsion used have maximal sensitivity. p and α were measured by our polarimeter to an accuracy of $\Delta p = \pm 1\%$ and $\Delta\alpha = \pm 2°$, respectively.

The noisiness n of a given α pattern (Table 3) was calculated as follows: the α patterns were scanned throughout with a window of 5 pixels × 5 pixels in which the standard variance (σ^2) of α was calculated, and then the average of the standard variances of all 5 pixel × 5 pixel windows was obtained. Finally, this value was normalized to that of white noise calculated with the same method. Thus, noisiness n of an α pattern denotes how noisy it is compared to the white noise ($n = 0\%$: no noise; $n = 100\%$: white noise).

The positions of the neutral points and the points of p extrema in the eclipsed sky were determined as follows: (i) in the inevitably noisy p patterns the regions of the local minima and maxima of p were detected after common Gaussian noise filtering. (ii) In these regions the pixels were determined where $p_{\text{local minimum}} \leq p \leq p_{\text{local minimum}} + 2\%$ and $p_{\text{local maximum}} - 2\% \leq p \leq p_{\text{local maximum}}$. (iii) The geometric centers of these pixels were calculated and defined as the positions of the local minima and maxima of p. (iv) In the case of the neutral points $p_{\text{local minimum}} = 0\%$–$1\%$ was taken.

3. Results

Figure 2 is a color photograph of the sky and the celestial patterns of p and α measured by full-sky

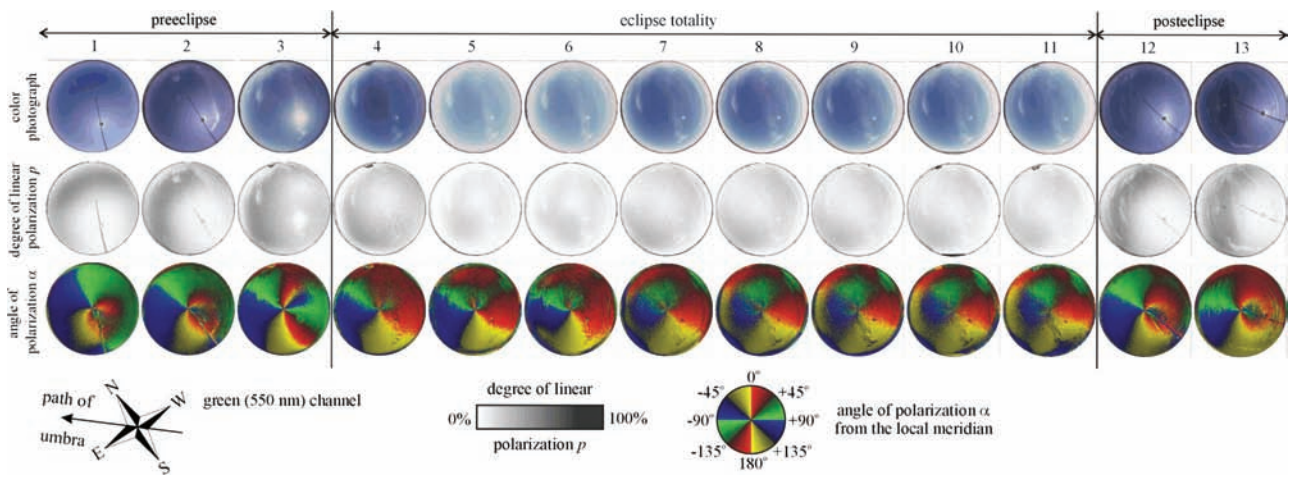

Fig. 2. (Color online) Photograph and patterns of the degree of linear polarization p and angle of polarization α of skylight measured by full-sky imaging polarimetry in the 550 nm spectral range during the total solar eclipse on 29 March 2006 in Turkey. The parameters of the recordings of scenes 1–13 are listed in Table 2. East (west) is at left (right) rather than on the right (left) of the compass rose, because we are looking up through the celestial dome rather than down onto a map.

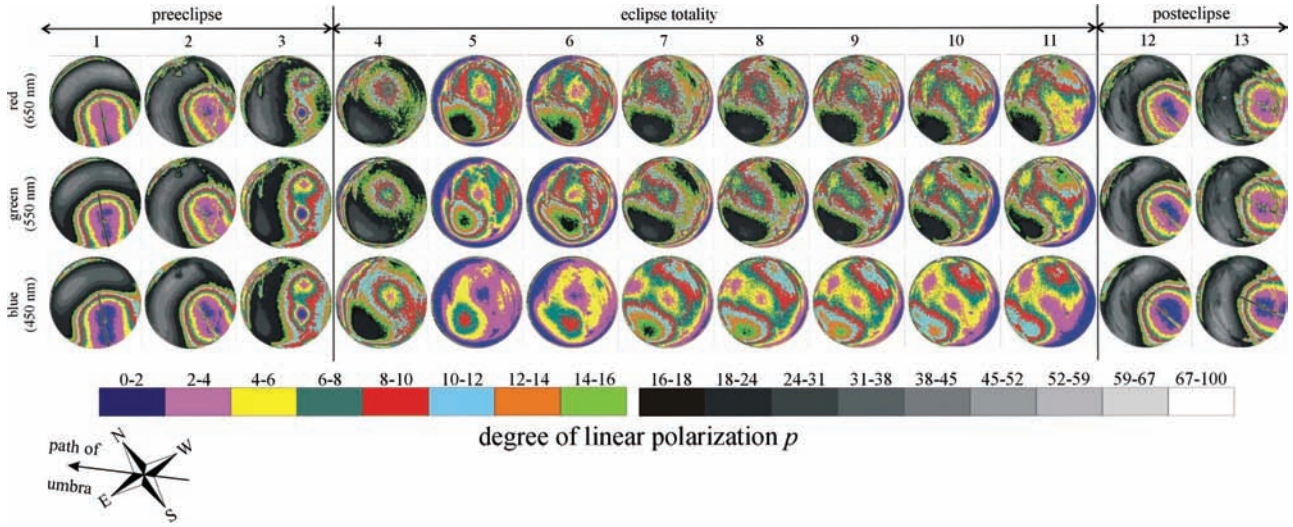

Fig. 3. (Color online) Patterns of p of skylight measured by full-sky imaging polarimetry in the 650 nm, 550 nm, and 450 nm parts of the spectrum during the eclipse on 29 March 2006 in Turkey. The parameters of the recordings of scenes 1–13 are listed in Table 2.

imaging polarimetry in the green (550 nm) spectral range during the total solar eclipse on 29 March 2006 in Turkey from the first to the fourth contact. Table 1 summarizes the most important parameters of this eclipse and the place of our measurements. Scenes 1 and 2 represent the sky conditions at the beginning (first contact) and the end (second contact) of the partial preeclipse, while scenes 12 and 13 represent the sky conditions at the beginning (third contact) and the end (fourth contact) of the partial posteclipse, respectively. Scene 3 with its 99.5% obscuration of the Sun's disk is an intermediate between the preeclipse and totality. The aim of Fig. 2 is to demonstrate an overview of what was happening in the sky during the eclipse. Note that the color pictures in Fig. 2 were taken at different exposure times, photoemulsions, and f numbers (Table 2), thus they do not represent the real temporal change of the celestial radiance. The color codes of the p and α values in Fig. 2 change gradually with small gray and color gradients. This color coding is ideal to represent the continuous spatial change of p and α of skylight, but it is disadvantageous if we want to visualize the local minima and maxima of p and the isolines of p and α (i.e., the lines for which the p and α values are constant). To eliminate this disadvantage of visualization, Figs. 3 and 4 represent the noise-filtered celestial p and α patterns measured in the red (650 nm), green (550 nm), and blue (450 nm) parts of the spectrum during the eclipse with the use of noncontinuous, discrete color codes. The relevant parameters of the recordings of scenes 1–13 in Figs. 2–4 are listed in Table 2. Table 3 contains the percentage k of the sky for which $45° \leq \alpha \leq 135°$ (shaded by green and blue colors in the α patterns), degree of polarization p, and noisiness n of the α pattern of the sky during the eclipse measured in the red, green, and blue parts of the spectrum and averaged for the entire sky.

During the preeclipse and the posteclipse both the p and the α patterns of the sky (scenes 1 and 2 and 12 and 13 in Figs. 2–4) were essentially the same as

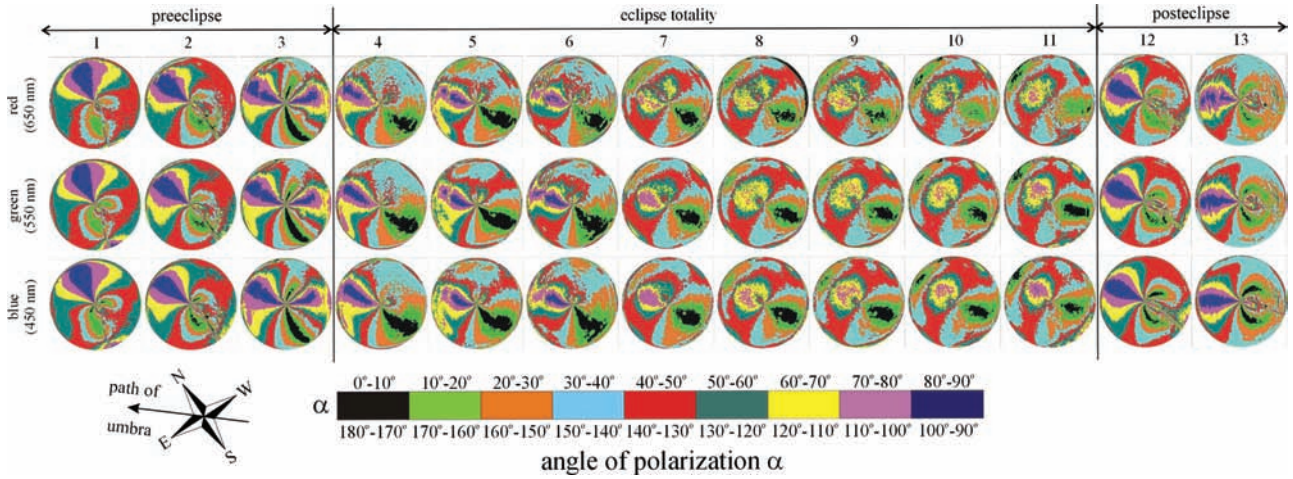

Fig. 4. (Color online) Same as Fig. 3 but for the angle of polarization α of skylight.

Table 4. Degree of Linear Polarization p (%) Measured by Full-Sky Imaging Polarimetry in the Red (R, 650 nm), Green (G, 550 nm) and Blue (B, 450 nm) Parts of the Spectrum at the Celestial Points with p Extrema in Scene 3 of the Preeclipse and in Scenes 4–11 of Totality During the Solar Eclipse on 29 March 2006 in Turkey[a]

	π_1			π_2			π_3			η_1			η_2		
Scene	R	G	B	R	G	B	R	G	B	R	G	B	R	G	B
Preeclipse															
3	41–43	27–29	27–29	27–29	20–22	20–22	—	—	—	4–6	2–4	2–4	6–8	6–8	6–8
Eclipse (totality)															
4	34–36	34–36	20–22	20–22	27–29	20–22	20–22	—	—	6–8	4–6	2–4	4–6	8–10	4–6
5	20–22	16–18	8–10	10–12	8–10	4–6	10–12	8–10	4–6	2–3	1–2	**0–1**	**0–1**	**0–1**	**0–1**
6	20–22	20–22	8–10	—	—	—	12–14	12–14	6–8	2–3	1–2	**0–1**	1–2	**0–1**	**0–1**
7	27–29	27–29	16–18	16–18	20–22	12–14	16–18	—	—	4–6	4–6	2–4	4–6	4–6	2–4
8	27–29	27–29	16–18	20–22	20–22	12–14	—	—	—	4–6	4–6	2–4	4–6	4–6	2–4
9	27–29	27–29	14–16	16–18	20–22	12–14	—	—	—	4–6	4–6	2–4	4–6	4–6	2–4
10	20–22	20–22	12–14	16–18	20–22	10–12	—	—	—	4–6	4–6	2–4	4–6	4–6	2–4
11	20–22	20–22	10–12	16–18	16–18	10–12	—	—	—	4–6	4–6	2–4	4–6	4–6	2–4

[a] π_1, π_2, π_3, local maxima of p; η_1, η_2, unpolarized (neutral) points (p = 0%–1%, bold) or local minima of p.

those of the normal clear sky, if the obscuration of the Sun's disk was not larger than 87.9% (preeclipse) and 88.5% (posteclipse): p of light from the preeclipse and posteclipse sky was always highest (depending on the wavelength and time with p_{max} = 45%–52%) at 90° from the Sun, and it gradually decreased toward the Sun and away from the Sun. Depending on the wavelength and time, $p_{average} + \Delta p$ was 30%–36% for the preeclipse and posteclipse skies, where Δp is the standard deviation of p. p was zero at the Babinet and Brewster neutral points positioned along the solar meridian at an angle of ~15° from the Sun. Depending on the wavelength and time, the percentage k of the α pattern for which $45° \leq \alpha \leq 135°$ was 57%–72% during the preeclipse, and 52%–57% at the beginning of the posteclipse. Hence, prior to and immediately after totality k was larger than 50%. Depending on the wavelength and time, the noisiness n of the celestial α pattern ranged from 8% to 15% during the preeclipse, and from 10% to 18% during the posteclipse. Both the p and the α patterns of the preeclipse and posteclipse skies were mirror symmetric to the solar–antisolar meridian. Apart from a slight rotation around the zenith due to the rotation of the solar meridian, the celestial polarization patterns were nearly constant during the preeclipse and posteclipse.

When the obscuration of the Sun's disk was 99.5%, considerable differences occurred between the polarization patterns of the preeclipsed sky and the normal sky, which are clearly seen in scene 3 of Figs. 2–4. Thus, scene 3 is an intermediate between preeclipse and totality, which is also reflected in the intermediate values of k, p, and n (Table 3).

During totality (when the obscuration of the Sun's disk was 100%) both the celestial p and the α patterns (scenes 4–11 in Figs. 2–4) were significantly different from those of the normal sky (scenes 1 and 2 and 12 and 13 in Figs. 2–4). The degrees of linear polarization of skylight were reduced relative to the p values of the preeclipse and posteclipse skies. Depending on the wavelength and time during totality, $p_{average} + \Delta p$ of skylight was 5%–26% (30%–36% for the preeclipse and posteclipse) and p_{max} = 4%–36% (45%–52% for the preeclipse and posteclipse), while k of the α pattern was 33%–43% (52%–72% for the preeclipse and posteclipse). Hence, during totality k was smaller than 50%. Depending on the wavelength and time, the noisiness n of the α pattern of the eclipsed sky ranged from 9% to 23%, values that are slightly larger than 8%–15% during the preeclipse and 10%–18% during the posteclipse. According to Figs. 2–4, during totality both the p and the α patterns of the sky changed more or less temporally, and the α pattern was approximately mirror symmetric to the solar–antisolar meridian.

During the preeclipse and totality, p of skylight was always lower in the blue spectral range than in the green and red parts of the spectrum (Tables 3 and 4). On the other hand, this trend was the opposite during the posteclipse: p became slightly higher in the blue than in the green and red, probably due to the enhanced amount of aerosols and haze in the afternoon atmosphere. Contrary to the relatively great dispersion of p of skylight, the wavelength dependence of α of skylight was rather modest during the entire eclipse period (from preeclipse through totality to posteclipse, Fig. 4).

During totality we observed some points with local minima or maxima of p (Figs. 5–8). Figure 5 shows the positions of the celestial points with p extrema in scenes 3–11 during the eclipse in the red, green, and blue spectral ranges. Figure 6 summarizes the temporal and spectral changes of the positions of these points of the eclipsed sky. Table 4 contains the p values measured in the red, green, and blue parts of the spectrum at the celestial points with p extrema in scenes 3–11 of the eclipse. In scenes 3–11 in all the red, green, and blue spectral ranges there were always two or three local maxima (π_1, π_2, and/or π_3), and two local minima (η_1 and η_2) of p. Both the positions and the minimal–maximal p values of the celestial points η_1, η_2, π_1, π_2, and π_3 depended

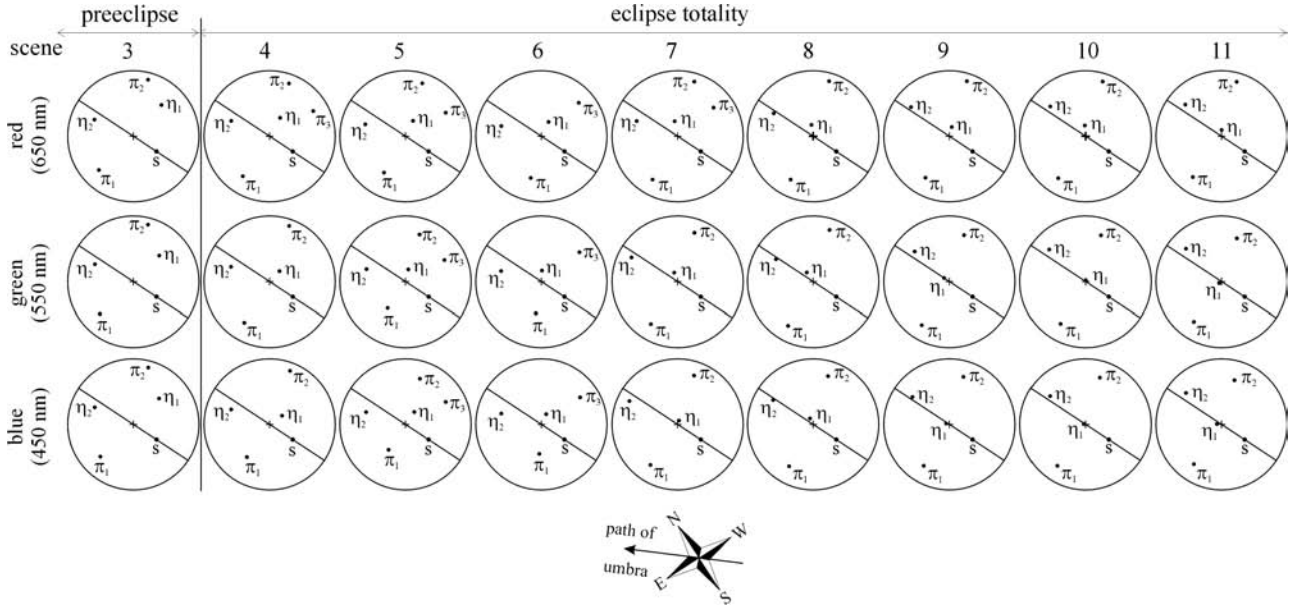

Fig. 5. Black dots represent the positions of the celestial points with p extrema in scenes 3–11 during the eclipse on 29 March 2006 in Turkey measured by full-sky imaging polarimetry in the R, 650 nm, G, 550 nm, and B, 450 nm parts of the spectrum π_1, π_2, π_3, local maxima of p; η_1, η_2, local minima of p; s, Sun; +, zenith; circle, horizon; diameter through the Sun, solar–antisolar meridian.

strongly on the wavelength of light (Table 4, Figs. 6–8).

The celestial points π_1, π_2, and π_3 with local maxima of p could be called "polarized points" in analogy to the "unpolarized (neutral) points." These polarized points were positioned near the horizon perpendicularly, and approximately symmetrical to the solar–antisolar meridian (Figs. 5 and 6). The position of the polarized point π_1 changed greatly in time, while the temporal variation of the positions of the other two polarized points π_2 and π_3 was small (Figs. 5 and 6). Figure 7 shows the change of p and α of skylight along a meridian passing through the celestial points π_1, π_2, and π_3 of scene 5 measured in the red, green, and blue parts of the spectrum. The two local maxima of p are clearly seen in the corresponding diagrams in Fig. 7.

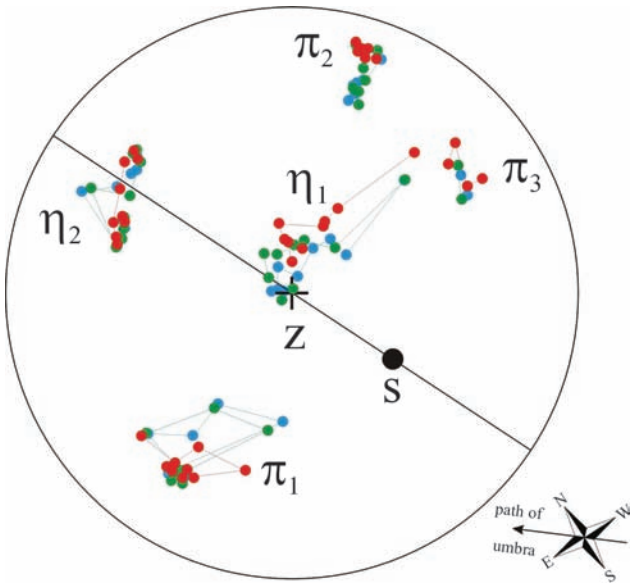

Fig. 6. (Color online) Same as Fig. 5 but here the dots represent the temporal and spectral changes of the positions of points π_1, π_2, π_3, η_1 and η_2 measured in the different parts of the spectrum and represented on the same celestial map. The zenith is indicated by z and its position by +.

Figure 8 shows the change of p and α of skylight along a meridian passing through the celestial points η_1 and η_2 of scene 5 measured in the red, green, and blue parts of the spectrum. The two local minima η_1 and η_2 of p are clearly seen in the diagrams in Fig. 8. One of the points (η_1) with a local minimum of p was near the zenith. The other local minimum of p (η_2) was near the horizon and the antisolar meridian (Figs. 5 and 6). According to Table 4 and Fig. 8, in scene 5 the local minimum η_2 of p ($\leq$1%) near the horizon may be a neutral point in all the red, green, and blue parts of the spectrum. The exact existence of such a neutral point is difficult to establish, because p was measured by our polarimeter to an accuracy of $\Delta p = \pm 1\%$. In scene 5 the local minimum η_1 of p ($\leq$1%) near the zenith could be a neutral point in the blue spectral range (Table 4, Fig. 8). Similarly, in scene 6 the local minimum η_2 of p ($\leq$1%) may be a neutral point in the green and blue parts of the spectrum, and the local minimum η_1 of p ($\leq$1%) could be a neutral point in the blue spectral range. The change of α is 90° if the neutral point η_1 near the zenith is crossed along the solar–antisolar meridian (Figs. 2, 4, and 8). Such a celestial point was classified as "type 2 neutral point" by Horváth *et al.* [16]. On the other hand, crossing the neutral point η_2 near the horizon, the wavelength-dependent change of α is much smaller than 90° (Figs. 2, 4, and 8). Horváth *et al.* [16] classified such a celestial point as "type 3 neutral

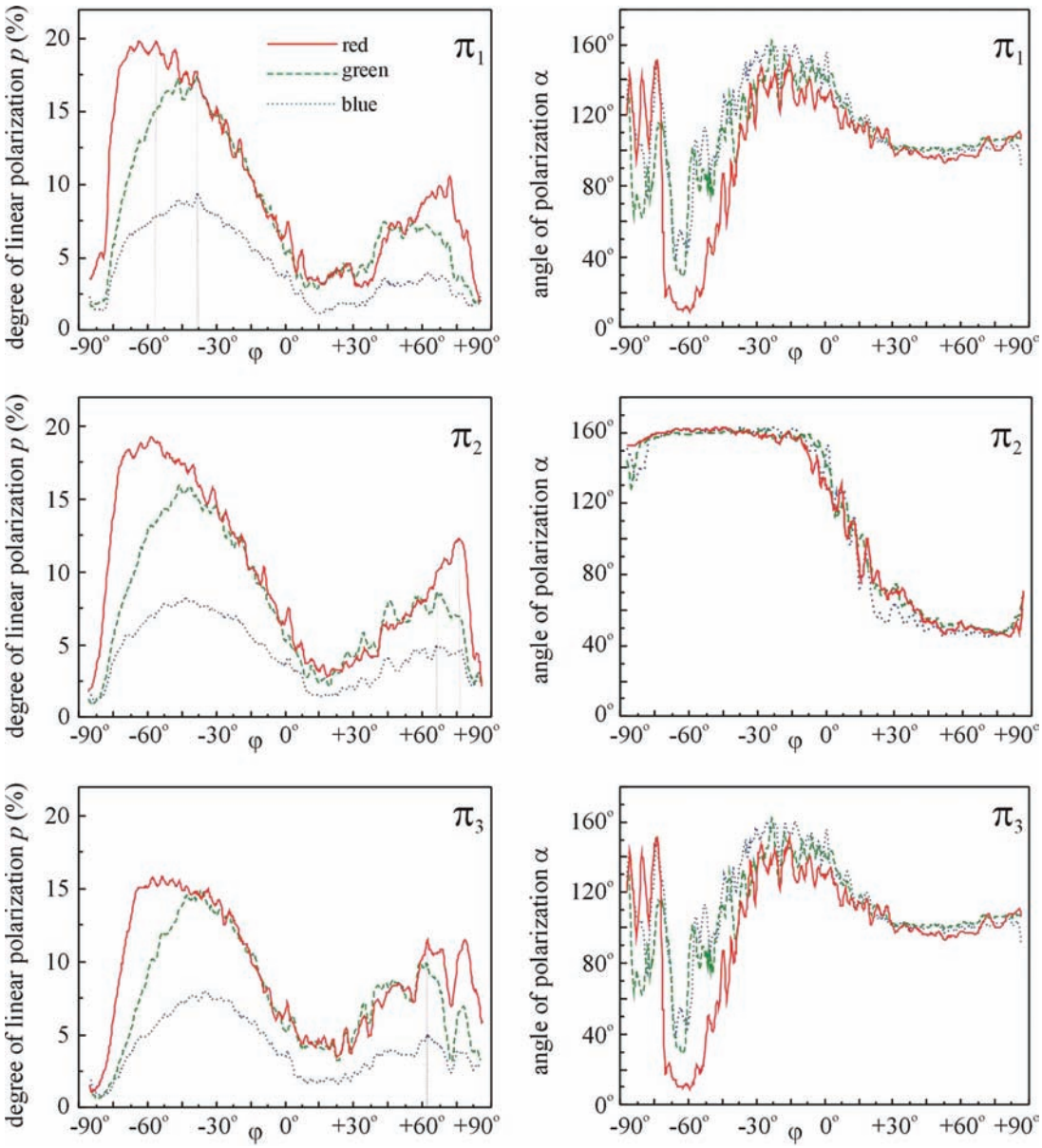

Fig. 7. (Color online) Change of p (left column) and α (right column) of skylight along a meridian passing through the celestial points π_1, π_2, and π_3 of scene 5 measured in the red, green, and blue parts of the spectrum (represented by red, green, and blue lines) during the eclipse on 29 March 2006 in Turkey. The horizontal axis shows the zenith angle φ (ranging from $-90°$ to $+90°$); the vertical axis represents either the p or the α values. The continuous vertical lines at left show the zenith angles of points with maximum p.

point." The position of point η_2 changed only slightly as a function of time, while the temporal variation of the position of point η_1 was considerable (Figs. 5 and 6).

4. Discussion

Pomozi *et al.* [15] and Horváth *et al.* [16] surveyed the earlier observations on sky polarization performed by point-source polarimetry during numerous different total solar eclipses [1–7,17]. Here we compare our results only with those of Pomozi *et al.* [15] and Horváth *et al.* [16], because only they used the same full-sky imaging polarimetric technique as we did in this work. We will see here that almost all the observations of Pomozi *et al.* [15] and Horváth *et al.* [16] were corroborated by our new observations during the eclipse on 29 March 2006 in Turkey. We would like to emphasize that the apparent discontinuity in α (that is the crossings of the isolines with α = constant) at the zenith is just a geometric artifact of the way α is defined in this work (α is measured from the local zenith meridian), rather than a true polarization singularity. For an alternative mapping of α see Berry *et al.* [18].

We found that during the preeclipse and posteclipse on 29 April 2006 the celestial polarization pattern was the same as that of the clear sky for obscurations of the Sun's disk not larger than 88.5%. The same results were obtained by Pomozi *et al.* [15] for obscurations of the Sun's disk not larger than 98% during the total solar eclipse of 11 August 1999 in

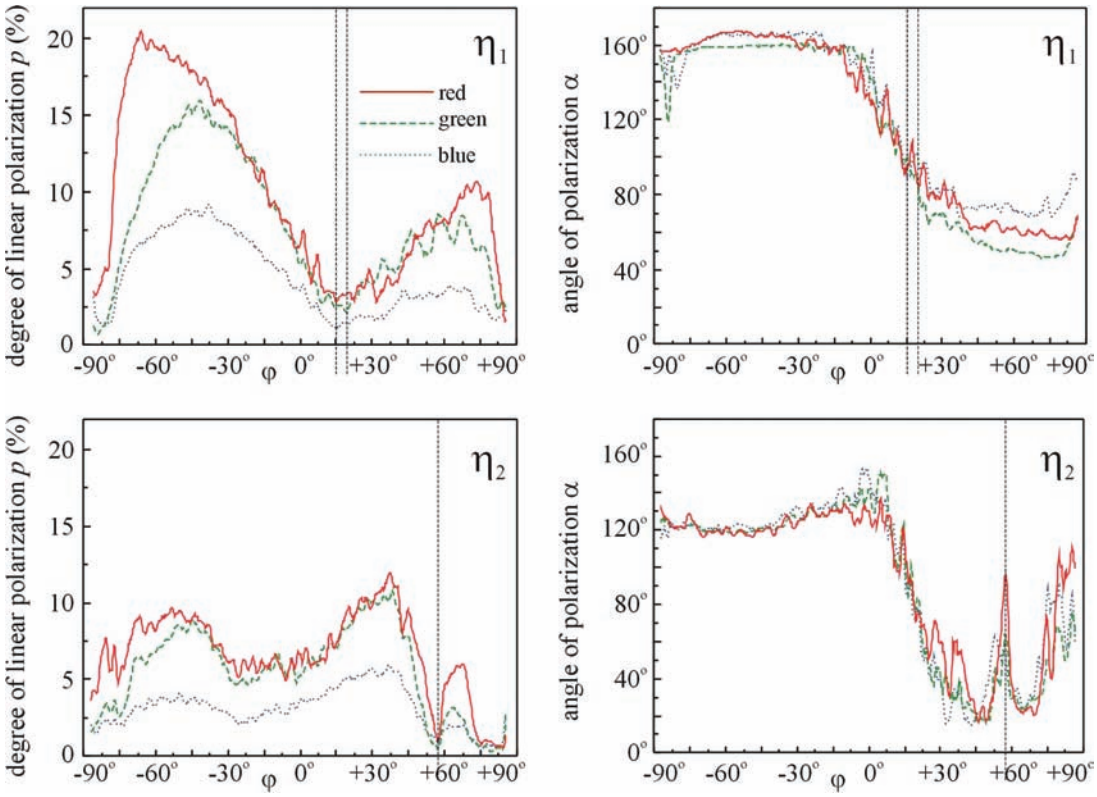

Fig. 8. (Color online) As Fig. 7 for the celestial points η_1 and η_2 of scene 5. The dashed vertical lines represent the zenith angles of points with minimum p.

Hungary. Coulson [8] observed the same effect during the partial solar eclipse on 26 February 1979 when the maximum obscuration of the Sun's disk was 80%. This means that, even if the obscuration is 98%, the polarization pattern of the eclipsed sky is predominantly determined by the scattering of sunlight coming directly from the eclipsed Sun's disk. However, according to our current observations, the polarization pattern of the eclipsed sky at 99.5% obscuration of the Sun's disk (scene 3 in Figs. 2–4) was considerably different from that of the normal and preeclipsed and posteclipsed skies. Hence, the polarization pattern of the sky suffers a sudden and dramatic change at the moment of the beginning and the end of the total eclipse, as observed by all earlier investigators [1–7,15–17].

During totality of the eclipse on 29 March 2006 in Turkey we could measure the polarization patterns of the sky at eight different points of time: six points of time before midtotality, and two points of time after midtotality (Table 2). The reason for the complex temporal change of the celestial polarization patterns observed during totality (Figs. 2–6) is that as the umbra (Moon's shadow) moved across the observation point, the geometry of light scattering changed due to the varying illumination conditions of the eclipsed sky. In Fig. 2 we can clearly see how the umbra passed above the observer: prior to mideclipse (scenes 4–7) the eclipsed sky was brightest on the left (northeast) half of the horizon, near mideclipse (scenes 8 and 9) the brightness distribution was nearly rotationally symmetric with respect to the zenith; after mideclipse (scenes 10 and 11) the eclipsed sky was brightest on the right (southwest) half of the horizon.

During the eclipse on 29 March 2006 in Turkey we observed approximately cylindrically symmetric p patterns only at scenes 4–7 (Figs. 2 and 3), that is prior to the midtotality, as also in the case of the eclipse studied by Pomozi *et al.* [15]. In the later phases of totality the celestial p pattern was not cylindrically symmetric, and striking p extrema developed (Figs. 2–8). Similarly to Pomozi *et al.* [15], we observed that during totality the α pattern was nearly mirror symmetrical to the solar–antisolar meridian. We also found that during the preeclipse and posteclipse the percentage k of the sky for which $45° \leq \alpha \leq 135°$ (shaded by green and blue colors in the α patterns) was larger than 50%, while during totality k became smaller than 50% (Table 3).

Similarly to Pomozi *et al.* [15], during the eclipse on 29 March 2006 we observed that during totality the skylight was the brightest and the darkest in the blue and red range of the spectrum, respectively. This can be explained by the Rayleigh scattering, which results in higher radiances of scattered light for shorter wavelengths and higher radiances of semidirect light for longer wavelengths. During totality semidirect light means the light that is scattered into the umbral area from the directly illuminated regions of the atmosphere outside the umbra. Furthermore, we also observed that during totality the longer the wave-

length of skylight, the higher was its p (Tables 3 and 4). Hence, during totality the wavelength dependence of p of light from the eclipsed sky is the same as that of light from the normal (noneclipsed) clear sky [8].

Similarly to Pomozi *et al.* [15] and Horváth *et al.* [16], during the totality of the eclipse on 29 March 2006 we also observed a neutral point η_1 near the zenith, and another neutral point η_2 near the horizon in the vicinity of the antisolar meridian (Table 4, Figs. 5, 6, and 8). In the zenith neutral point $p = 0$, and farther away from it p gradually increased. Crossing this neutral point along the solar–antisolar meridian, α suffered a sudden change of 90°. The Arago, Babinet, Brewster, and the fourth neutral points of skylight polarization possess similar characteristics [8,19,20].

On the basis of the comparison between the observations on 11 August 1999 in Hungary (with a zenith angle of 32° of the eclipsed Sun) and on 29 March 2006 in Turkey (with a solar zenith angle of 46°), we conclude that the above-mentioned characteristics of the polarization patterns of the eclipsed sky seem to be general, rather than specific. The validity of this conclusion drawn from the results gathered during two different eclipses should be tested by further imaging polarimetric observations of future total solar eclipses.

The equipment donation of the German Alexander von Humboldt Foundation received by Gábor Horváth is acknowledged. We thank Rüdiger Wehner (Zoological Institute, University of Zurich, Switzerland) who lent his Nikon fish-eye lens to us for our imaging polarimetric measurements. Many thanks for the valuable and constructive comments of two anonymous reviewers.

References

1. N. Piltschikoff, "Sur la polarisation du ciel pendant les éclipses du soleil," C. R. Acad. Sci. **142,** 1449 (1906).
2. E. de Bary, K. Bullrich, and D. Lorenz, "Messungen der Himmelsstrahlung und deren Polarisationsgrad während der Sonnenfinsternis am 15.2.1961 in Viareggio (Italian)," Geofis. Pura Appl. **48,** 193–198 (1961).
3. J. G. Moore and C. R. N. Rao, "Polarization of the daytime sky during the total solar eclipse of 30 May 1965," Ann. Geophys. **22,** 147–150 (1966).
4. C. R. N. Rao, T. Takashima, and J. G. Moore, "Polarimetry of the daytime sky during solar eclipses," J. Atmos. Terr. Phys. **34,** 573–576 (1972).
5. B. S. Dandekar and J. P. Turtle, "Day sky brightness and polarization during the total solar eclipse of 7 March 1970," Appl. Opt. **10,** 1220–1224 (1971).
6. R. E. Miller and W. G. Fastie, "Skylight intensity, polarization and airglow measurements during the total solar eclipse of 30 May 1965," J. Atmos. Terr. Phys. **34,** 1541–1546 (1972).
7. G. E. Shaw, "Sky brightness and polarization during the 1973 African eclipse," Appl. Opt. **14,** 388–394 (1975).
8. K. L. Coulson, *Polarization and Intensity of Light in the Atmosphere* (Deepak, 1988).
9. G. P. Können, "Skylight polarization during a total solar eclipse: a quantitative model," J. Opt. Soc. Am. A **4,** 601–608 (1987).
10. J. A. North and M. J. Duggin, "Stokes vector imaging of the polarized sky-dome," Appl. Opt. **36,** 723–730 (1997).
11. K. J. Voss and Y. Liu, "Polarized radiance distribution measurements of skylight. I. System description and characterization," Appl. Opt. **36,** 6083–6094 (1997).
12. Y. Liu and K. J. Voss, "Polarized radiance distribution measurements of skylight. II. Experiment and data," Appl. Opt. **36,** 8753–8764 (1997).
13. J. Gál, G. Horváth, V. B. Meyer-Rochow, and R. Wehner, "Polarization patterns of the summer sky and its neutral points measured by full-sky imaging polarimetry in Finnish Lapland north of the Arctic Circle," Proc. R. Soc. London Ser. A **457,** 1385–1399 (2001).
14. G. Horváth, A. Barta, J. Gál, B. Suhai, and O. Haiman, "Ground-based full-sky imaging polarimetry of rapidly changing skies and its use for polarimetric cloud detection," Appl. Opt. **41,** 543–559 (2002).
15. I. Pomozi, J. Gál, G. Horváth, and R. Wehner, "Fine structure of the celestial polarization pattern and its temporal change during the total solar eclipse of 11 August 1999," Remote Sens. Environ. **76,** 181–201 (2001).
16. G. Horváth, I. Pomozi, and J. Gál, "Neutral points of skylight polarization observed during the total eclipse on 11 August 1999," Appl. Opt. **42,** 465–475 (2003).
17. R. Gerharz, "Appearance of the atmospheric scatter field during a solar eclipse," J. Geophys. **42,** 163–167 (1976).
18. M. V. Berry, M. R. Dennis, and R. L. Lee, Jr., "Polarization singularities in the clear sky," New J. Phys. **6,** 162 (2004).
19. G. Horváth, B. Bernáth, B. Suhai, A. Barta, and R. Wehner, "First observation of the fourth neutral polarization point in the atmosphere," J. Opt. Soc. Am. A **19,** 2085–2099 (2002).
20. G. Horváth and D. Varjú, *Polarized Light in Animal Vision—Polarization Patterns in Nature* (Springer-Verlag, 2003).